

Published in final edited form as:

*Am J Physiol.* 1986 January ; 250(1 Pt 2): H29–H42.

## Multiple tracer dilution estimates of D- and 2-deoxy-D-glucose uptake by the heart

JYRKI KUIKKA, MICHAEL LEVIN, and JAMES B. BASSINGTHWAIGHTE

Center for Bioengineering, University of Washington, Seattle, Washington 98195; and  
Department of Clinical Physiology, University Central Hospital, SF-70210 Kuopio, Finland

### Abstract

Permeability-surface area products of the capillary wall,  $PS_c$ , and the myocyte sarcolemma,  $PS_{pc}$ , for D-glucose and 2-deoxy-D-glucose were estimated via the multiple indicator-dilution technique in isolated blood-perfused dog and Tyrode-perfused rabbit hearts. Aortic bolus injections contained  $^{131}\text{I}$ -albumin (intravascular reference), two of three glucoses: L-glucose (an extracellular reference solute), D-glucose, and 2-deoxy-D-glucose. Outflow dilution curves were sampled for 1–2.5 min without recirculation. The long duration sampling allowed accurate evaluation of  $PS_{pc}$  by fitting the dilution curves with a multiregional axially distributed capillary-interstitial fluid-cell model accounting for the heterogeneity of regional flows (measured using microspheres and total heart sectioning). With average blood flow of  $1.3 \text{ ml}\cdot\text{g}^{-1}\cdot\text{min}^{-1}$ , in the dog hearts the  $PS_c$  for D-glucose was  $0.72 \pm 0.17 \text{ ml}\cdot\text{g}^{-1}\cdot\text{min}^{-1}$  (mean  $\pm$  SD;  $n = 11$ ), and  $PS_{pc}$  was  $0.57 \pm 0.15 \text{ ml}\cdot\text{g}^{-1}\cdot\text{min}^{-1}$ . In the rabbit hearts with perfusate flow of  $2.0 \text{ ml}\cdot\text{g}^{-1}\cdot\text{min}^{-1}$  ( $n = 6$ ),  $PS_c$  was  $1.2 \pm 0.1$  and  $PS_{pc}$  was  $0.4 \pm 0.1 \text{ ml}\cdot\text{g}^{-1}\cdot\text{min}^{-1}$ .  $PS_c$  for 2-deoxy-D-glucose was about 4% higher than for D-glucose and L-glucose in both preparations. Relative to L-glucose, there was no measurable transendothelial transport of either dextroglucose, indicating that transcapillary transport was by passive diffusion, presumably via the clefts between cells. The technique allows repeated measurements of D-glucose uptake at intervals of a few minutes; it may therefore be used to assess changes in transport rates occurring over intervals of several minutes.

### Keywords

isolated heart preparation; coronary transport function; myocardial transsarcolemmal flux; L-glucose; dogs; rabbits

---

THERE HAS BEEN A substantial accumulation of data from isolated heart preparations and in vitro muscle preparations on the utilization of D-glucose by myocardium, as, for example, in the symposium edited by Opie (20). The data provided on glucose utilization have been estimated in these many studies from the arteriovenous differences or from the diminution in glucose concentration in the perfusate or in the bathing medium, and in earlier studies by estimating the glycogen formation. Lacking in these studies was knowledge of the unidirectional transsarcolemmal influx of glucose, a value that is independent of the net transsarcolemmal flux and that is needed to characterize the transport mechanism in normal or in compromised states. Crone (8) showed that the indicator-dilution technique was applicable, indeed invaluable, for the estimation of glucose permeability of the blood-brain barrier and in his studies showed that permeation was via a saturable facilitated transport mechanism. In the heart there are two membranes to consider, the capillary and the sarcolemmal membranes, making the analysis complex. The multiple-tracer indicator-

dilution technique provides a suitable vehicle for measuring unidirectional transsarcolemmal uptake rates in laboratory and potentially for clinical situations. The analysis requires incorporating mathematical solutions for capillary-tissue units accounting for capillary and cell barriers to exchange, such as that of Goresky and his colleagues (29), as components of a multicapillary model accounting for flow heterogeneity.

The practical incentives to gain fundamental insight into the rates of transcapillary and transsarcolemmal transport of D-glucose have been much increased by the use of [ $^{18}\text{F}$ ]fluorodeoxyglucose; its relative regional deposition density in the heart can be estimated by positron emission tomographic reconstruction (24). With the appropriate analysis it should be possible to estimate regional transsarcolemmal uptake rates in the hearts of intact animals or humans, which would be a practical extension of the autoradiographic approach of Sokoloff et al. (33).

Our current studies were designed to provide estimates of cellular D-glucose uptake by comparison with a set of reference tracers of partially analogous characteristics. The three reference tracers were 1)  $^{131}\text{I}$ -albumin, which is a reference tracer for transport in the blood plasma; 2) L-glucose, which has the same molecular weight as D-glucose (mol wt = 180) and which this study shows to have the same capillary permeability-surface area product ( $PS_c$ ) as D-glucose; it serves as an extracellular reference tracer; its interstitial fluid (ISF)

volume of distribution ( $V'_{\text{ISF}}$ ) is the same as for sucrose (unpublished data) and presumably for D-glucose, and it does not participate in the facilitated transport available for most D-glucoses (15, 22); and 3) 2-deoxy-D-glucose (mol wt = 164), which is transported across cell membranes via the same carrier as D-glucose but which is not metabolized to  $\text{CO}_2$  and  $\text{H}_2\text{O}$ . On entering the cells, 2-deoxy-D-glucose, like D-glucose, is phosphorylated via hexokinase to form 2-deoxy-D-glucose-6-phosphate but, unlike glucose, cannot be transformed to glucose 1-phosphate form by phosphoglucomutase, nor to fructose 6-phosphate via the isomerase, and so cannot be metabolized through the glycolytic series. The 2-deoxy-D-glucose phosphate is neither soluble in the membrane, nor transported outward via a carrier, nor dephosphorylated very rapidly, since there is little or no glucose phosphatase in the heart, and it is therefore retained by the cells for a long time; these features have led to its use as an indicator of cellular glucose uptake and, by inference, metabolism. These factors, plus the fact that 2-deoxy-D-glucose will not necessarily be transported into the cell at the same rate as D-glucose, mean that a comparison of the kinetics of these two glucoses is useful.

Studies were undertaken mainly in blood-perfused dog hearts and in three Tyrode-perfused rabbit hearts. In these preparations we have acquired data on the transcapillary transport of glucose and of its analogues. The general principles of the experimentation and analyses are given by Bassingthwaite and Goresky (3). The analysis is strengthened over previous efforts by virtue of the use of a new optimization technique by which the three dilution curves in a set are fitted simultaneously with the model solutions. This reduces the degrees of freedom in the parameter estimation and so provides more accurate estimates but could not be automated on our present computer system with limited memory, so it is left as an example of an improvement to be put into standard practice at a later time.

## Experimental Methods

### Indicator-Dilution Technique

Both dog and rabbit hearts were studied. Eighteen sets of dilution curves were obtained on isolated, Langendorff, nonworking, spontaneously beating hearts. The dog hearts were perfused with blood at  $37.5^\circ\text{C}$  taken from the femoral artery of an anesthetized, artificially

ventilated support dog weighing about 30 kg, as described in detail previously (11). The support dogs were fasted overnight; blood glucose levels were not measured. The rabbit hearts were perfused with oxygenated Tyrode solution through an aortic cannula. The perfusate composition was (mM) Na 147.4, K 5.4, Ca 1.8, Mg 0.5, Cl<sup>-</sup>133.1, HCO<sub>3</sub><sup>-</sup>23.8, H<sub>2</sub>PO<sub>4</sub><sup>-</sup>0.4, EDTA 0.01, and glucose 5 and was without albumin. The temperature of circulating solutions was maintained at 37.5–38°C, and 23 sets of dilution curves were obtained.

The perfusion rate was controlled with a roller pump on the inflow line. Perfusion pressure, perfusate temperature, coronary sinus pressure, heart rate, and heart weight were monitored and recorded continuously. Drainage from the coronary sinus, right atrium, and right ventricle was collected via a tapered cannula through the right ventricular free wall near the apex. The left ventricular Thebesian vein inflow plus aortic valve leakage were drained via a small cannula through the apex. Flows through the right and left ventricular cannulas were measured, and venous samples were collected for hematocrit and blood glucose determinations before injection of tracers and periodically thereafter. The arterial and perfusion pressures, sampling time, and heart rate were continuously recorded. At the end of each experiment, the wet weight of the myocardium devoid of fatty tissue was measured.

**Injections**—The timing of the injections into the arterial inflow, lasting 1.0–2.0 s for dog hearts and 0.5–1.0 s for rabbit hearts, was recorded, and the midpoint was used as zero time ( $t = 0$ ). The injectate contained an intravascular reference substance, albumin, and two of the three test substances. The radioactive tracers were diluted with physiological saline or Tyrode solution; the volume of the injectate was 2.9 ml for dogs and 0.2–0.5 ml for rabbits.

**Tracers**—The following radiotracers were used: 1) <sup>131</sup>I-RIHSA (radioiodinated human serum albumin as a reference intravascular tracer), 2) 2-deoxy-D-[1-<sup>3</sup>H]glucose, 3) D-[6-<sup>3</sup>H]glucose, 4) D-[1-<sup>14</sup>C]glucose, and 5) L-[1-<sup>14</sup>C]-glucose as an extracellular reference solute (all supplied by Amersham Radiochemical Center, London, UK). Three injection mixtures were prepared: 1) 2-deoxy-D-[1-<sup>3</sup>H]glucose + L-[1-<sup>14</sup>C]glucose + <sup>131</sup>I-RIHSA, 2) D-[6-<sup>3</sup>H]glucose + L-[1-<sup>14</sup>C]glucose + <sup>131</sup>I-RIHSA, and 3) 2-deoxy-D-[1-<sup>3</sup>H]glucose + D-[1-<sup>14</sup>C]glucose + <sup>131</sup>I-RIHSA. The activities used were 40 μCi of <sup>3</sup>H-labeled tracer, 20 μCi of <sup>14</sup>C-labeled tracer, and 10 μCi of <sup>131</sup>I-RIHSA for dog experiments, and 4, 2, and 1 μCi, respectively, for rabbit experiments. Radiochemical purity of these five tracers were tested by using paper chromatography; the results showed 98% purity for <sup>131</sup>I-RIHSA and for L-glucose and 99% purity for the D-glucose and deoxyglucose.

**Sampling**—The blood and Tyrode samples were collected from the coronary sinus outflow (right ventricle) at intervals of 0.4–1.0 s for the first 30 samples and 2–4 s for the last 30 samples, depending on the flow rate used. The total collection period was 72–150 s. A volume of 0.1 ml of each outflow sample, each standard, and each background sample was pipetted into scintillation vials. For the blood samples, the proteins were precipitated with 0.1 ml of 70% perchloric acid and 0.2 ml of 30% hydrogen peroxide, and the vials were heated at 100° Celsius for 1 h. Ten milliliters of scintillation cocktail (Insta-Gel, Packard Instrument, Downers Grove, IL) were added for both the dog and rabbit samples.

**Radioisotope activities**—Counting was done in a liquid scintillation counter (Nuclear Chicago, Mark II, Searle) using three channels. Four sets of quench correction curves (background, <sup>3</sup>H-, <sup>14</sup>C-, and <sup>131</sup>I-labels) of 35 data points each were made for both dog and rabbit experiments. The “best” least-squares polynomials were fitted to the quench-data points, and the polynomials were used to estimate the true counting rates of the <sup>3</sup>H-, <sup>14</sup>C-, and <sup>131</sup>I-labels of each sample.

To test the accuracy of the sampling and counting methods, two D-glucoses ( $^3\text{H}$ - and  $^{14}\text{C}$ -labeled) were injected simultaneously with  $^{131}\text{I}$ -RIHSA in one dog experiment. The dilution curves obtained for these D-glucoses should theoretically be identical. The analysis of samples showed an excellent agreement; the mean absolute difference between the  $^3\text{H}$ - and  $^{14}\text{C}$ -samples was 0.74%, and the correlation coefficient between the 54 sample points was 0.999992.

**Calculation of dilution curves**—The dilution curves contained relatively little statistical counting noise, since the peak counting rate was usually higher than 100,000 counts/10 min for each tracer. The reference curve was terminated at 0.1–0.01% of the peak and the glucose curves at 1.0–0.1% of the peak (no recirculation), so that counting errors ordinarily had standard deviations less than 3% and spillover corrections (using a Gaussian elimination technique to invert the matrix) added very little more, as demonstrated by the test with the two D-glucoses. Each dilution curve was normalized so that it is the “transport function” of the system from injection site to sampling site,  $h(t)$ , which is the fraction of dose appearing in the venous outflow per second

$$h(t) = F_B C(t) / q_0 \quad (1)$$

where  $F_B$  is the flow of blood or perfusate through the coronary bed (ml/s),  $q_0$  is the quantity of tracer injected ( $\mu\text{Ci}$ ), and  $C(t)$  is outflow concentration of the tracer in the effluent at time  $t$  ( $\mu\text{Ci/ml}$ ). Our notation is  $h_R(t)$  for a reference intravascular tracer and  $h_D(t)$  for any permeating or diffusible tracer. From these, one may calculate an apparent instantaneous extraction  $E(t)$  at each point:  $E(t) = 1 - h_D(t)/h_R(t)$ .  $E_{\max}$  is the maximum of  $E(t)$  after smoothing, as defined by Guller et al. (11) and occurs at about the time of the peak of  $h_R(t)$ .

### Estimation of Flow Heterogeneity from Microsphere Deposition

**Microsphere injections**—In some, but not all, experiments, microspheres were injected into the aortic cannula to obtain an estimate of the heterogeneity of regional flows, as described by Yipintsoi et al. (36), using 9- $\mu\text{m}$  diameter spheres labeled with  $^{85}\text{Sr}$  or  $^{46}\text{Sc}$  (3M, St. Paul, MN). Previous experiments on dogs (36) and baboons (14) show that these distributions change very little over many minutes in experiments with varying blood flows, so there is little need for injecting the microspheres and the diffusible tracers simultaneously. Two microsphere injections were made:  $^{85}\text{Sr}$  after the first or second injection of diffusible tracers and  $^{46}\text{Sc}$  after the third or fourth tracer injection. The volumes injected were 1 ml for dogs and 0.2 ml for rabbits, and the activities used were 1–3  $\mu\text{Ci}$  and 0.05–0.1  $\mu\text{Ci}$ , respectively. The total number of microspheres was 3–20  $\times 10^5$  for dogs and 0.1–4  $\times 10^5$  for rabbits, or 5,000–25,000 microspheres/g of heart.

**Microsphere deposition densities**—At the end of each dog experiment the heart was cooled on dry ice and sliced into 10 major sections, the atria, 4 right ventricular rings, and 5 left ventricular rings, and then into 297 finer sections, ordered as described by King et al. (14). The rabbit hearts were sliced similarly but into fewer pieces. The weight of the heart pieces ranged between 0.03 and 0.19 g. The radioactivity of each piece was determined by multichannel gamma counting, as described in detail by King and Bassingthwaite (13). For each heart, the probability density function of regional microsphere activity was constructed; it was interpreted as equivalent to the probability density function of regional myocardial flows.<sup>1</sup>

<sup>1</sup>For the methods of computation available in detail, order NTIS Document UW/BIOENG-82/1 from National Technical Information Services, Dept. of Commerce, 5285 Port Royal Rd., Springfield, VA 22161.

The probability density function of microspheres (regional flows) per gram of tissue is given by a weighting function  $w(f)$ , where the probability  $w$  is a function of the relative flow,  $f$ , and where  $f$  is defined as the local flow per unit mass of tissue divided by the measured mean flow per unit mass. In histogram notation, the relative flow in the  $i^{\text{th}}$  class is  $f_i$ , and the fraction of the organ having flows within the class centered at  $f_i$  is  $w_i \Delta f_i$ . The sum of the  $w_i \Delta f_i$  is unity, to account for the whole heart. The tracer enters each of the  $i$  regions in proportion to flow, i.e., the  $i^{\text{th}}$  region of relative mass  $w_i \Delta f_i$  receives the fraction  $f_i w_i \Delta f_i$  of the tracer. The sum of the  $f_i w_i \Delta f_i$  is unity, accounting for all of the flow.

## Methods of Analysis

For the analysis, the heart was described by an aggregate of capillary-tissue units in parallel. Each unit was a three-region (capillary, ISF, cell), two-barrier, axially distributed convection-diffusion model. A basic assumption is that diffusion in the radial direction (perpendicular to the capillary axis) is rapid compared with the transmembrane transport processes, which is justifiable because the intraregional radial distances are so short; intercapillary distances are less than  $20 \mu\text{m}$ . The model is an extension of the one-barrier model of Bassingthwaite (2) and is conceptually similar to the two-barrier model of Rose, Goresky, and Bach (29). Its virtues are the speed and stability of computation, providing solutions to fit to data extending over long durations such as many minutes or hours. Parameters of the model for fitting the dilution curves are as follows:

1.  $F_s$ , mean flow of solute-containing mother fluid ( $\text{ml} \cdot \text{g}^{-1} \cdot \text{min}^{-1}$ ) =  $F_B(1 - \text{Hct})$   
(From data:  $F_B$  is blood flow and Hct is hematocrit)
2. Heterogeneity of flows, given by the probability density function of microsphere deposition densities,  $w_i$  and  $f_i$ , dimensionless. The standard deviation of this density function divided by the mean is the relative dispersion of regional flows, RD. The local perfusate flow in the  $i^{\text{th}}$  region is  $f_i F_s = F_{s_i}$ . (For the multicapillary analysis the density function was represented by 5 or 7 regions, rather than the 25 classes into which the microsphere deposition densities had been partitioned)
3.  $PS_c$ , capillary permeability-surface area product,  $\text{ml} \cdot \text{g}^{-1} \cdot \text{min}^{-1}$
4.  $\gamma_{\text{ISF}}$ , dimensionless ratio of interstitial volume of distribution,  $V'_{\text{ISF}}$  (ml/g), to the intracapillary volume of distribution,  $V'_c$  of the particular tracer
5.  $PS_{\text{pc}}$ , permeability-surface area product of parenchymal cell (of sarcolemma of myocytes),  $\text{ml} \cdot \text{g}^{-1} \cdot \text{min}^{-1}$
6.  $\gamma_{\text{pc}}$ , dimensionless ratio of the volume of tracer distribution within parenchymal cell,  $V'_{\text{pc}}$ , to the intracapillary volume of distribution,  $V'_c$
7.  $G_{\text{pc}}$ , clearance rate for intracellular sequestration or consumption,  $\text{ml} \cdot \text{g}^{-1} \cdot \text{min}^{-1}$   
[ $G_{\text{pc}}/V'_{\text{pc}}$  is  $k_5$  in the notation of Rose, Goresky, and Bach (29)]

The differential equations for the system in each capillary-interstitial fluid-cell unit are

$$\begin{aligned} \frac{\partial C_c(x,t)}{\partial t} &= \left[ \frac{F_{s_i} L}{V'_c} \right] \frac{\partial C_c}{\partial x} - \frac{PS_c}{V'_c} [C_c - C_{\text{ISF}}] + D_c \frac{\partial^2 C_c}{\partial x^2} \\ \frac{\partial C_{\text{ISF}}(x,t)}{\partial t} &= \frac{PS_c}{V'_{\text{ISF}}} [C_c - C_{\text{ISF}}] - \frac{PS_{\text{pc}}}{V'_{\text{ISF}}} [C_{\text{ISF}} - C_{\text{pc}}] + D_{\text{ISF}} \frac{\partial^2 C_{\text{ISF}}}{\partial x^2} \quad (2) \\ \frac{\partial C_{\text{pc}}(x,t)}{\partial t} &= \frac{PS_{\text{pc}}}{V'_{\text{pc}}} [C_{\text{ISF}} - C_{\text{pc}}] - \frac{G_{\text{pc}}}{V'_{\text{pc}}} C_{\text{pc}} - D_{\text{pc}} \frac{\partial^2 C_{\text{pc}}}{\partial x^2} \end{aligned}$$

The subscripts are C for capillary, ISF for interstitium, and pc for parenchymal cell (myocyte). In addition to the parameters listed above, the other symbols are  $C_c$ ,  $C_{\text{ISF}}$ , and

$C_{pc}$  for concentrations (counts/min per ml volume of distribution in each region) at position  $x$  at time  $t$ ;  $x$  is distance along the capillary from the entrance at  $x = 0$  to the exit at  $x = L$ .  $D_C$ ,  $D_{ISF}$ , and  $D_{pc}$  are axial diffusion coefficients; intracapillary diffusion has a small influence on the form of the dilution curves during the first 1–2 s following the appearance time; for glucose, with its low transport rate, diffusion has no discernible effect on the estimates of the other parameters, and the  $D$ s were set to zero for this analysis. A fast numerical method (5), using the Lagrangian sliding fluid element approach of Bassingthwaite (2) was used to obtain solutions to the equations, solved for each pathway with individual values for  $F_{si}$ . Its accuracy, with axial diffusion, was evaluated by Lenhoff and Lightfoot (16) for a two-region solution and found to be within 1% of that of an analytic solution for the same model. The unit impulse response at the outflow from the  $i^{\text{th}}$  region is  $h_{Ci}(t)$ ; note, however, that the model was used as a differential operator, thus avoiding convolution integration.

With  $PS_C$  zero, the indicator remains intravascular and has a mean transit time  $\bar{t} = V'_c/F_s$ .

With  $PS_C > 0$ , and  $PS_{pc} = 0$ , the indicator remains extracellular, with  $\bar{t} = (V'_c + V'_{ISF})/F_s$ .

With  $PS_C$  and  $PS_{pc}$ , both  $> 0$  and  $G_{pc} = 0$ ,  $\bar{t} = (V'_c + V'_{ISF} + V'_{pc})/F_s$ . The effect of  $G_{pc} > 0$  is to shorten  $\bar{t}$  compared with the nonconsumed tracer with the same volume of distribution, because there is a greater fraction consumed in slow flow regions and at late times when the tracer is largely inside the parenchymal cell where the consumption occurs.

An aggregate of these capillary-tissue units plus large vessel units made up the whole heart model. The aggregate of parallel capillary-tissue units gives the overall transport function of the capillary exchange regions  $h_C(t)$ , using the flow weighting obtained from the microsphere distributions

$$h_C(t) = \sum_i w_i f_i \Delta f_i h_{Ci}(t) \quad (3)$$

For an individual tracer all units have the same parameters except for  $F_{si}$ . The various diffusible tracers were allowed to have different values for  $PS$  and  $V$  in the initial analyses.

The capillary-tissue units were considered to be in series with large vessels which also disperse and delay the tracers as described by the large vessel transport functions  $h_{LV}(t)$ . The convolution of the set of capillary transport functions with a single large vessel transport function is appropriate when the large vessel dispersion is similar for all capillary-tissue regions. This gives the overall model transport function  $\hat{h}(t)$  as a convolution (denoted by the asterisk) of  $h_{LV}$  and  $h_C$

$$\hat{h}(t) = h_{LV}(t) * h_C(t) \quad (4)$$

Rose, Goresky, and Bach (29) used a heterogeneity model of a different form, having a set of dispersionless large vessels also in parallel and linking them via a 1:1 linear relationship to the capillaries. Their model has not been compared with ours but could give different parameter estimates.

**Optimization of the fits of the model to the data**—Two new approaches have been used in the analysis. First, the method of optimization of the parameter values to achieve a good fit of the model to the data is a new one based on the use of the sensitivity functions (17). Second, the degrees of freedom in the parameter evaluation are reduced strongly by fitting several components of a set of data (flows, dilution curves, and microsphere deposition densities) simultaneously with a multicomponent model.

The nature of sensitivity functions and their use was introduced by Levin, Kuikka, and Bassingthwaite (17) but will be summarized here. Sensitivity functions,  $S_p(t)$ , are defined as partial derivatives of the model solution with respect to each of the parameters of interest,  $p$ , as a function of time

$$S_p(t) = \frac{\partial \hat{h}(t)}{\partial p} \quad (5)$$

where  $p$  is any of the parameters,  $PS_C$ ,  $\gamma_{ISF}$ ,  $PS_{pc}$ ,  $\gamma_{pc}$ , and  $G_{pc}$ . The caret denotes a model solution, as opposed to the observed dilution curve. The sensitivity functions for these parameters are shown in Fig. 1 for a representative model solution. Mathematical independence of the parameters is demonstrated by the fact that no sensitivity function is a scalar or a reciprocal of another.

For each free parameter there is a unique  $S_p(t)$  that differs from those of other parameters it describes the extent by which the model solution  $\hat{h}(t)$  would be increased by an increase in the parameter value. Thus for example, the influence of increasing  $PS_C$  on  $\hat{h}_D(t)$  is to reduce its height at early times, as indicated by  $S_{PS_C}$  being negative. At a time late in the washout phase when  $h_D(t)$  is higher than  $h_R(t)$ , an increase in  $PS_C$  results in an increase in  $\hat{h}_D(t)$ , so that  $S_{PS_C}$  is positive at late times. Although parameters are independent, there are interactions between them. Our optimization technique is based on the principle that their relative influences are different at each time  $t$  and that for each there is a period when its influence is maximal. The distance (with its negative or positive sign) between the model  $\hat{h}_D(t)$  and the data  $h_D(t)$  around a particular time of maximal influence of one parameter gives information via the sensitivity functions on how much to change all of the free parameters.

For example, consider a hypothetical case where there are three free parameters, with the sensitivity functions for each. (For 5 parameters, the technique is identical, but discussing 3 is briefer.) The influences of parameters,  $PS_C$ ,  $\gamma$ ,  $PS_{pc}$  have their maxima at times  $t_1$ ,  $t_2$ , and  $t_3$ , i.e., the absolute values of the three sensitivity functions are relatively large at these times. But at each time there is some influence of all three parameters. The difference between the model functions  $\hat{h}(t_1)$  and the observed  $h(t_1)$ , at a particular time  $t_1$ , can be related to the values of the sensitivity functions at the same time  $t_1$  via an approximating linear equation containing three unknowns, the changes in parameter values, the  $\Delta p$ 's, required to get a better fit at this time point. Similarly one would need other equations for other particular times. With two other times;  $t_2$  and  $t_3$ , there are three equations with three unknowns

$$\begin{aligned} h(t_1) - \hat{h}(t_1) &= \Delta PS_C \cdot S_{PS_C}(t_1) + \Delta \gamma \cdot S_\gamma(t_1) + \Delta PS_{pc} \cdot S_{PS_{pc}}(t_1) \\ h(t_2) - \hat{h}(t_2) &= \Delta PS_C \cdot S_{PS_C}(t_2) + \Delta \gamma \cdot S_\gamma(t_2) + \Delta PS_{pc} \cdot S_{PS_{pc}}(t_2) \\ h(t_3) - \hat{h}(t_3) &= \Delta PS_C \cdot S_{PS_C}(t_3) + \Delta PS_{pc} \cdot S_{PS_{pc}}(t_3) \end{aligned} \quad (6)$$

This can be written as an array of differences,  $D$ , where  $D_1 = h(t_1) - \hat{h}(t_1)$ , etc., and  $PS_C$  is parameter 1,  $p_1$ ;  $\gamma$  is  $p_2$ ;  $PS_{pc}$  is  $p_3$ ; and the sensitivity function value for  $p_1$  at  $t_1$  is  $S_{11}$ , etc., giving

$$\begin{aligned} D_1 &= \Delta p_1 S_{11} + \Delta p_2 S_{12} + \Delta p_3 S_{13} \\ D_2 &= \Delta p_1 S_{21} + \Delta p_2 S_{22} + \Delta p_3 S_{23} \\ D_3 &= \Delta p_1 S_{31} + \Delta p_2 S_{32} + \Delta p_3 S_{33} \end{aligned} \quad (7)$$

This matrix was solved for the best estimates of  $\Delta PS_C$ ,  $\Delta\gamma$ , and  $\Delta PS_{pc}$  by a standard matrix inversion technique, Gaussian elimination. The new parameter values are the previous values plus the changes, the  $\Delta p$ 's.

In practice, time windows were used instead of single time points; these were short time spans around each maximum point of  $S_X(t)$ .  $D_1$ , for example, represented an area between  $\hat{h}(t)$  and  $h(t)$  for several seconds around  $t_1$ , divided by the duration of the period. By this mechanism the influence of particular data points is reduced, and the effect of noisy data is minimized. In addition, when the sensitivity function for one parameter is changing sign near time  $t_1$ , the influence on this parameter is quite properly reduced toward zero.

With this optimization technique, one is not minimizing any global distance function such as a sum of squares or coefficient of variation but rather is matching model to data in sets of local regions that are defined by the sensitivity functions. The search ceases when the gradients no longer change or if the coefficient is less than 1%. The coefficient of variation (CV) that we report uses all the data points and therefore provides a global measure of the goodness of fit achieved but is not the function being minimized: it is  $CV = [\sum(\hat{h}_i - h_i)^2 / (n - 1)]^{1/2} / (\sum \hat{h}_i / n)$ , where the index  $i$  denotes the value of  $h$  or  $\hat{h}$  at time  $t_i$ , and  $n$  is the number of data points in the curve.

**Reduction of degrees of freedom**—Greatest accuracy in parameter estimation is achieved when the degrees of freedom are minimal, given that the model is physiologically appropriate.  $PS_C$  for albumin is assumed to be zero, which is appropriate for the short times involved in these studies; the albumin curve, the measured mean flow, the distribution of regional flows (from microsphere data), and an assumed capillary volume,  $V'_c$  of 0.035 ml/g (6), thereby completely define the large vessel transport function,  $h_{LV}(t)$ , which is obtained by deconvolution in accordance with Eq. 4. This  $h_{LV}(t)$  is used as the input function for the three  $h(t)$ s in each set;  $h_R(t)$  should, and does automatically, give an exact fit to the observed  $h_R(t)$  when the axial diffusion coefficient is set to zero. Recruitment with increasing flow, a physiological possibility, is not an issue since the  $PS$ s for the three glucoses were obtained in pairs without changing flow, nor is the assumption of a particular value for  $V'_c$ . Any other value from 0.005 to 0.5 would do as well, since the analysis determines  $PS/F$ , and  $F$  is measured experimentally.

For L-glucose only two parameters,  $PS_C$  and  $\gamma_{ISF}$ , were free. While there might otherwise be five free parameters for D-glucose and deoxyglucose, in practice these two were fixed when L-glucose was one of the three tracers injected:  $PS_C$  was the same for D- as for L-glucose;  $PS_C$  for deoxyglucose was  $(180/164)^{1/2}$  ( $=1.048$ , the expected ratio of free aqueous diffusion coefficients, proportional to the square root of the ratio of mol wts) times that for L-glucose (assuming permeation without significant steric hindrance);  $V'_{ISF}$  was the same for each pairing of the three glucoses. When D- and 2-deoxy-D-glucose were paired, both  $\gamma_{ISF}$  and  $\gamma_{pc}$  were the same for both sugars, but  $PS_C$  and  $PS_{pc}$  were unconstrained. The results will show that the ratio of  $PS_C$  for D- to deoxyglucose was not statistically different from 1.048, verifying the use of the assumption for L-glucose, as well as indicating the absence of substantial transcapillary escape via the plasmalemma of the endothelial cells.

## RESULTS

### Experimental Outflow Dilution Curves

The dog heart weights ranged from 102 to 230 g, and the rabbit hearts from 7.6 to 10.6 g. Perfusion pressures were 50–120 mmHg in dogs, 40–130 in rabbits. Heart rates were from 50 to 90  $\text{min}^{-1}$  in dogs, 60–140 in rabbits. None of these appeared to influence the estimates

of the parameters. The mean coronary flows and their relative dispersions (from the microsphere data) are given for the dog studies in Table 1 and for the rabbits in Table 2.

Experimental outflow dilution curves are shown in Fig. 2 and given in numerical form in Table 3. The paired D- and L-glucose dilution curves were essentially identical during the upslope and peak of the curves. From this we conclude that the transport rates for D- and L-glucose across the capillary wall are identical. Because L-glucose does not enter cells (except very slowly), we conclude further that endothelial luminal surface uptake of D-glucose is negligible and infer that both D- and L-glucose permeate via passive diffusion through aqueous channels, presumably the clefts between endothelial cells.

The curves differed during the washout phase. The difference was small, even though no fatty acid was available in the perfusate in the rabbit experiments. In the later phase of washout both the D- and 2-deoxy-D-glucose curves often, but not always, become closer to and then cross above the L-glucose curve paired with it. This pattern is consistent with the reflux of tracer from the cells through the ISF to the effluent perfusate.

### Influences of Parameter Values on Model Solutions

From the similarity of the D- and L-glucose curves in Fig. 2 one can see that capillary  $PS_C$  and the initial back diffusion from ISF must be the same for D- and L-glucose. These effects are shown by the sensitivity functions in Fig. 1 to occur early, while cellular effects occur later.

The influences of  $PS_{pc}$  and  $G_{rc}$ , on the dilution curve, shown in Fig. 3, are all on the tails of the curves and not on the unslope and peaks. Figure 3A shows the effects of increasing rates of permeation into the myocytes, in an artificial situation in which there is no reflux from the cell. The absence of cellular efflux is equivalent to having an infinite intracellular consumption,  $G_{pc}$ , or an infinite intracellular volume of distribution,  $V'_{pc}$ . With intermediate values of  $PS_{pc}$  from 0.25 to 8 ml·g<sup>-1</sup>·min<sup>-1</sup>, the height of the peak of  $h_D(t)$  is little affected, but the height of the tail beyond  $t = 20$  s is greatly reduced by cellular influx in the absence of efflux. With both  $V'_{pc}$  and  $PS_{pc}$  very high, the ISF concentration is held at zero and there is no return flux from cell or ISF to the capillary. Then in the  $i^{\text{th}}$  pathway the transport function for the permeating tracer,  $h_{D_i}(t)$ , has a shape identical to that of the intravascular reference,  $h_{R_i}(t)$ , but scaled down according to the local capillary permeability and local flow

$$\frac{h_{D_i}(t)}{h_{R_i}(t)} = e^{-PS_c / F_{s_i}} \quad (8)$$

This condition of no back diffusion from ISF to capillary is the hypothetical basis of the classic Crone-Renkin expression for estimating capillary permeability, although these authors considered only one capillary. The composite outflow dilution curve  $h_D(t)$  is the weighted sum of the individual  $h_{D_i}(t)$ s, as in Eq. 3; its shape is different from that of the  $h_R(t)$  because the fraction of tracer taken up by the cells is greater in low-flow pathways than high-flow pathways, in accordance with the early, rising value of the instantaneous extraction  $E(t)$  in Fig. 1.

Allowing bidirectional flux across the cell membrane (Fig. 3B) gives an improved fit to the D-glucose curve. The curve for  $PS_{pc} = 0$  is the best fit to the simultaneously obtained L-glucose curve. Initially the curves for  $PS_{pc} = 0$  and 0 are the same, but they separate on the downslope. Later, return flux from the cell results in the model D-glucose curve crossing

above L-glucose (that for  $PS_{pc} = 0$ ), a marked difference from the behavior in Fig. 3A, where the separation increases.

Figure 3C shows that consumption or sequestration within the cell reduces the return flux from the cell and the mean transit time of the outflow curve. During the 1st min the effect on  $\hat{h}_D(t)$  of increasing  $G_{pc}$  is the same as enlarging  $V'_{pc}$ . Later, the effects differ in that an enlarged  $V'_{pc}$  gives reflux later, whereas chemical reaction gives rise to metabolite species. Within the 2 min of data collection in these experiments, the difference between reversible binding and reaction cannot be ascertained accurately. Constraining the values of  $V'_{pc}$  to the neighborhood of the known intracellular water space reduces the variability of estimates of  $G_{pc}$ .

The effect of intracellular consumption on the amount and time course of untransformed tracer-labeled substrate emerging in the outflow dilution curve is greater when the rate of entry into the cell is higher; when  $PS_C$  and  $PS_{pc}$  are higher, sensitivity to  $G_{pc}$  is higher. The effect of  $G_{pc}$  is always to reduce return flux of untransformed tracer into the outflow. At high values of  $G_{pc}$  all intracellular tracer is consumed, and the curves are the same as for zero reflux (Fig. 3A). Thus the key to the unraveling of the relative effects of the various parameters on the model solutions to be fitted to the data is that each parameter influences different parts of the outflow dilution curves in different ways so that each parameter has a unique influence on the curve, independent of all of the other parameters. That this should occur is indicated by differences between the sensitivity functions shown in Fig. 1.

### Parameter Values Estimated from Dilution Curves

The data for the blood-perfused dog hearts and for the Tyrode-perfused rabbit hearts fall into two separate ranges of perfusate flow. The higher viscosity and lower “plasmacrit” in the dog studies result in lower flows than in the rabbit experiments. Even so, the flows in our dog studies are still on the average higher than normal flows in dog hearts at rest. High flows are desirable only from the point of view of obtaining accurate estimates of  $PS_C$  and  $\gamma_{ISF}$ . Lower flows and even longer total sampling durations would have helped in estimating  $\gamma_{pc}$  and  $G_{pc}$ .

In Tables 1 and 2 are listed the parameter values resulting from the fitting of the models to the experimental curves from dog and rabbit hearts. An example of solutions fitted to a D-glucose curve in a rabbit heart is shown in Fig. 3. Model solutions for D- and 2-deoxy-D-glucose are shown from a dog heart in Fig. 4. In the optimization  $\gamma_{ISF}$  was forced to have the same value for each of the pair of permeant tracers. This takes advantage of the physiological expectation that D-, L-, and 2-deoxy-D-glucose should have the same volume of distribution in the ISF and also reduces the number of free parameters and gives a more reliable estimate of  $\gamma_{ISF}$  (which is  $V'_{ISF}/V'_c$ ). Each of the two glucose models in a run has the same flow heterogeneity, the same vascular volumes,  $V'_c$  and the same interstitial volumes  $V'_{ISF}$ .

$PS_{pc}$ , for L-glucose was fixed at zero, in accord with its role as an extracellular reference tracer. Although this is the expected value, since L-glucose is reported not to enter cells (9, 19, 21), a preliminary set of analyses was done on the L-glucose curves with  $PS_{pc}$ , free to vary. The result was that the estimates of  $PS_{pc}$  for L-glucose were very low, usually less than  $0.05 \text{ ml}\cdot\text{g}^{-1}\cdot\text{min}^{-1}$ , and the confidence intervals calculated from the optimization almost always included zero. Therefore, there was no clear evidence for a nonzero value of  $PS_{pc}$ , for L-glucose. In studies on awake rabbits in our laboratory we estimated the intracellular concentration of tracer-labeled L-glucose ( using sucrose as reference) was less than 3% of

the plasma concentration 30 min after intravenous injection. Therefore, in the subsequent analyses,  $PS_{PC}$  for L-glucose was fixed at zero, reducing the degrees of freedom in fitting the pairs of glucose curves with the dual model.

A further logical restriction was to assume that the values for  $PS_C$  were proportional to their free diffusion coefficients over the 5% range involved here, namely to set  $PS_C$  for D-glucose equal to that of L-glucose and to fit  $PS_C$  for deoxyglucose at 1.048 times that for L-glucose. When these constraints were set aside in the interest of seeing what results would emerge from the unbiased estimates of  $PS_C$ , the goodness of fit of the models to the data was only negligibly improved, indicating that the constraining was not only useful in reducing the degrees of freedom, but that there was no evidence that the basic assumption might be wrong.

### Estimates of $PS_C$

The values of  $PS_C$  for blood-perfused dog hearts were lower than for the Tyrode-perfused rabbit hearts. The ratios of deoxyglucose to D-glucose were  $1.042 \pm 0.02$  ( $n = 8$  in 5 dogs and 3 rabbits), close to the expected ratio, 1.048. Thus the  $PS_C$ s for these glucoses are apparently in proportion to their free diffusion coefficients in water. For D-glucose the mean value of  $PS_C$  was  $0.72 \pm 0.17$  ( $n = 11$ ) for dog myocardial capillaries and  $1.15 \pm 0.14$  ( $n = 6$ ) for rabbit myocardial capillaries when Tyrode perfused. For 2-deoxy-D-glucose,  $PS_C$  in dog hearts averaged  $0.80 \pm 0.22$  ( $n = 12$ )  $\text{ml}\cdot\text{g}^{-1}\cdot\text{min}^{-1}$  and in three rabbit hearts  $1.2 \pm 0.2$  ( $n = 3$ ). Values for L-glucose are not reported in Tables 1 or 2: when paired with D-glucose,  $PS_C$  (L-glucose) and  $PS_C$  (D-glucose) were defined as equal and the best value determined for the pair; when 2-deoxy-D-glucose and L-glucose were paired,  $PS_C$  (deoxyglucose)/ $PS_C$  (L-glucose) was fixed at 1.048. In dog hearts the mean  $PS_C$  (L-glucose) was  $0.69 \pm 0.22$  ( $n = 13$ )  $\text{ml}\cdot\text{g}^{-1}\cdot\text{min}^{-1}$  and in rabbit hearts  $1.2 \pm 0.1$  ( $n = 3$ ), the higher value in rabbits probably being attributable to the lack of albumin in the perfusate.

A test of adequacy of the conclusion that the  $PS_C$ s were in proportion to free diffusion coefficients is given by Fig. 5 in which their ratios were fixed. Three sets of dilution curves from one dog study, nine  $h(t)$ s, obtained in sequence without changing the flow were fitted with four free parameters only: one degree of freedom for  $PS_C$ , one for  $V'_{ISF}$ , and two for  $PS_{PC}$ . The value for  $V'_{PC}$  was fixed at  $\gamma_{PC} = 12.5$  ( $V'_{PC} = 0.44$   $\text{ml/g}$ ), about an average value from the analyses summarized in Tables 1 and 2.  $G_{PC}$  for D-glucose and 2-deoxy-D-glucose was fixed from an approximate calculation from a steady-state extraction of 5% to be  $0.2$   $\text{ml}\cdot\text{g}^{-1}\cdot\text{min}^{-1}$  (see DISCUSSION following Eq. 12). The results in Fig. 5, A–C, show that in spite of the reduction of degrees of freedom to 4 instead of 24 (2 for each L-glucose curve, 5 for each of the 4 dextroglucose curves), the fitting of the model solutions to the data are quite good, particularly in the first 20–30 s in which  $PS_{PC}$ , and  $G_{PC}$  have less influence; the overall coefficient of variation for the 6 glucoses was 0.11. The conclusion is that the constraining is useful and acceptable in obtaining good estimates of  $PS_C$ ; such approaches could therefore have been used on other triple sets of data, but this mode of analysis is left for future studies when it can be automated. Logical constraining of  $PS_C$  and  $V'_{ISF}$  (or  $\gamma_{ISF}$ ) should probably be used more generally, since the result will be more accurate estimates of the parameters which should be left free,  $PS_{PC}$  and  $G_{PC}$ .

### Estimates of $V'_{ISF}/V'_C$

Values for  $\gamma_{ISF}$ , or  $V'_{ISF}/V'_C$ , ranged from 3.7 to 7.8 with a mean of  $5.4 \pm 1.2$  ( $n = 18$ ) in dogs (Table 1) and from 7.9 to 10.0 with a mean of  $9.0 \pm 0.7$  ( $n = 6$ ) in the Tyrodeperfused rabbit

hearts (Table 2), which are ordinarily moderately edematous. Using  $V'_c = 0.035$  ml/g, in dogs  $V'_{ISF} = 0.0035 \times 5.4 \approx 0.19$  ml/g and in rabbits  $V'_{ISF} \approx 0.30$  ml/g.

### Estimates of $PS_{pc}$

Values for  $PS_{pc}$  for d- and 2-deoxy-D-glucose are given in Tables 1 and 2. The estimates are apparently independent of the flow, over a range of mean myocardial plasma flow from 0.41 to over 2.0 ml·g<sup>-1</sup>·min<sup>-1</sup> in dogs and from 1.7 to 2.8 in rabbits. Since intercapillary diffusion distances are small enough, 17–22 μm, so that diffusional equilibration times locally over regions with these diameters are small, 10–60 ms, the rate of equilibration within the ISF is rapid compared with transmembrane transport rate constants, such as  $PS_{pc}/V'_{ISF}$ . This means that all of the parenchymal cell surface is quickly exposed to a more or less uniform extracellular concentration ( $C_{ISF}$ ) even if only every other capillary is open. Thus constancy of  $PS_{pc}$  in the presence of some flow effect to recruit capillaries implies that recruitment occurs within neighboring groups of capillaries, as was observed by Rose et al. (29).

### Estimates of $V'_{pc}/V'_c$

Estimates of  $V'_{pc}/V'_c$  or  $\gamma_{pc}$  can be made from the outflow dilution curves when there is reflux of tracer from cells to outflow. L-glucose is not useful in this regard since it does not enter cells. D-glucose and 2-deoxy-D-glucose are phosphorylated via hexokinase, and only the unphosphorylated form can exit from the cell, so estimates of  $\gamma_{pc}$  are less accurate than if  $G_{pc}$  were zero. (Following this argument, one might choose 3-*O*-methylglucose, which is presumably not reacted with inside the cell, as a good indicator for measuring  $\gamma_{pc}$ , but this was not a primary goal here). Presumably the phosphorylated forms are too polar to traverse the membrane. In the absence of a significant phosphatase reaction in the cell (hydrolyzing the phosphate), it follows that any reflux of deoxyglucose implies the persistence of unphosphorylated glucose or deoxyglucose at a finite concentration within the cell. The estimates of  $\gamma_{pc}$  from D-glucose and 2-deoxy-D-glucose averaged  $12.7 \pm 0.94$  ( $n = 18$ ) in dog hearts and  $10.1 \pm 2.1$  ( $n = 6$ ) in rabbit hearts, or about 0.44 and 0.35 ml/g for  $V'_{pc}$ . The mere fact that reasonable volumes are estimated indicates that intracellular concentrations are finite. See DISCUSSION.

The total of the volumes of distribution,  $V'_c + V'_{ISF} + V'_{pc}$  or  $V'_c (1 + \gamma_{ISF} + \gamma_{pc})$ , was about 0.67 ml/g in dogs and 0.70 in rabbits; both are less than the total water space. This is mainly because the large vessel volume (~0.1 ml/g) is excluded from the computation. If one were to consider the large vessel volume to be zero, then the result could suggest that the arbitrary choice of  $V'_c = 0.035$  was too small; a value of 0.0406 ml/g for  $V'_c$  would give a total water space of 0.777 ml/g, the water space of dog hearts (37). Since large vessel volumes are not zero, a value of 0.0406 is an overestimate of  $V'_c$ , and the anatomic estimate of 0.035 (6) is physiologically reasonable. Affirming this argument, the sum of the large vessel volume, 0.1 ml/g, plus the total intratissue volume of distribution, 0.67 ml/g, is 0.77 ml/g, almost the expected value of 0.777 ml/g.

### Estimates of $G_{pc}$

$G_{pc}$  represents a rate of clearance from the cell cytoplasm into a pool from which there is no return to the cytoplasm. The accuracy of estimation of  $G_{pc}$  is reduced whenever  $PS_{pc}$  is low, as it is here. The dog data curves were analyzed with  $\gamma_{pc}$  and  $G_{pc}$  free; the estimates of  $G_{pc}$  for D-glucose were  $0.2 \pm 0.3$  ml·g<sup>-1</sup>·min<sup>-1</sup> ( $n = 11$ ) and for deoxyglucose were  $0.2 \pm 0.4$  ( $n = 12$ ). The estimates are obviously imprecise but are compatible with calculations from

arteriovenous differences and estimates of glucose consumption [e.g., from Rovetto et al. (30)].

## DISCUSSION

### Importance of Heterogeneity of Flows

Taking into account the heterogeneity of regional myocardial blood flows is critical to the accurate estimation of parameter values. Comparisons between multicapillary and single capillary analysis showed that  $PS_C$  would be underestimated by 2–50% if a single capillary model were used.  $PS_{pc}$  would be estimated with less than 20% error either if  $PS_{pc}$  were less than  $1 \text{ ml}\cdot\text{g}^{-1}\cdot\text{min}^{-1}$  or if the heterogeneity of flow were less than 25%, given that  $PS_C$  is greater than  $F_S/2$ . At higher values of relative dispersion, greater than 25% or with estimates of  $PS_{pc}$  greater than  $1 \text{ ml}\cdot\text{g}^{-1}\cdot\text{min}^{-1}$ , overestimates of  $PS_{pc}$  could be as large as threefold. In actuality, estimates for  $PS_C$  using a three-region axially distributed single-capillary model were  $21\% \pm 12\%$  ( $n = 36$  curves in dog hearts) less than those obtained using the multicapillary model. The estimates of  $PS_{pc}$  were on the average quite similar for both single and multicapillary modeling; the ratio (single/multiple) was  $0.87 \pm 0.28$  ( $n = 21$ ). The smallness of the error was due to two offsetting errors: errors in  $PS_C$  due to single-capillary modeling led to errors in  $PS_{pc}$  that were opposite in direction to those occurring when only  $PS_{pc}$  is free to err.

### Capillary Permeability-Surface Area Products

Most of the data available in the literature on estimating  $PS_C$  has been obtained by use of the Crone-Renkin equation

$$PS_C \text{ (Crone)} = -F_S \log_e(1 - E_{\max}) \quad (9)$$

where  $E_{\max}$  is the apparent maximal extraction during the upslope and the time of the peak of the indicator-dilution curves (cf. Eq. 8). This formula does not account for return flux of tracer from ISF into the effluent blood and so gives an underestimate of the unidirectional flux from the capillary plasma across the capillary membrane into the interstitium. Accordingly, from our data the estimates of  $PS_C$  (Crone) from this equation averaged  $79 \pm 14\%$  ( $n = 36$ ) of the estimates obtained from the multicapillary modeling, which we consider to be the current “gold standard.”

As anticipated from this result, our estimates averaging  $0.72 \text{ ml}\cdot\text{g}^{-1}\cdot\text{min}^{-1}$  for  $PS_C$  are therefore somewhat higher than those obtained for the heart by earlier investigators. Values of  $PS_C$  for glucose in isolated, blood-perfused, nonworking dog hearts obtained by Alvarez and Yudilevich (1) were  $0.31 \pm 0.09 \text{ ml}\cdot\text{g}^{-1}\cdot\text{min}^{-1}$  ( $n = 14$ ), by Yipintsoi et al. (38) were  $0.31 \pm 0.13$  ( $n = 23$ ), and by Duran and Yudilevich (10) at the highest flows were  $0.64 \pm 0.09$  ( $n = 11$ ), all of which can be interpreted as underestimates because of lack of accounting for tracer reflux from ISF to capillary (“back diffusion”). In rabbit hearts perfused with Krebs-Henseleit solution, Bassingthwaight et al. (4) found a correction factor for the calculation of the “true  $PS_C$ ” for ascorbate and glucose from the  $PS_C$  (Crone); i.e., true  $PS_C = 1.39 PS_C$  (Crone), with a standard deviation of 34%. The dog data of this study would suggest a smaller error

$$\text{True } PS_C = 1.30 PS_C \text{ (Crone)} \quad (10)$$

with a standard deviation of 18% ( $n = 26$ ). There is a good reason for the difference, namely that blood-perfused hearts, with substantially lower  $PS_C$ s, have smaller errors because there is less back diffusion. One can expect the error in the Crone expression to be larger with larger values of  $PS_C/F_S$ , as Cousineau et al. (7) observed.

We should emphasize that the data on  $PS_C$  for the dogs and those from rabbits do differ significantly, the rabbit having the higher values. This is presumably partly due to the absence of albumin in the perfusate for the rabbit hearts and also to the presence of higher flows and virtually complete vasodilation. The isolated Tyrode-perfused rabbit heart is certainly not a normal physiological preparation in that the  $PS_C$  is abnormally high, although it seems otherwise to be a perfectly adequate model for testing our methods of analysis and for studying a variety of phenomena in which interstitial edema does not interfere.

Having concluded that glucose is transported passively via clefts across myocardial capillaries, one may contrast this with the situation at the tight endothelial barrier in the brain. For blood-brain exchange the present models would have to be augmented to include another barrier and concentration-dependent permeabilities. Transport across brain capillaries is by a facilitated, or carrier-mediated, transport mechanism (8), and the transcapillary conductances  $PS_C$  are concentration dependent. The conductance for tracer is governed by the concentration of nonlabeled glucose at each point in the capillary in each particular steady state; the steady state is not changed by the presence of tracer so Eqs. 2 are appropriate locally, but the  $PS$ s change by even a quarter or a third, increasing as concentrations of nontracer diminish toward the capillary outflow. Brain capillary  $PS_C$  is not low because of the carrier facilitation (8, 39), and the degree of underestimation by the Crone-Renkin expression (Eq. 9) may not be any less than in the heart.

### Estimation of $V'_{ISF}$

The true volume of the ISF space,  $V_{ISF}$ , can be estimated from  $\gamma_{ISF}$  (from the modeling), the hematocrit, and the assumed total capillary volume of the heart of 0.035 ml/g (6)

$$V'_{ISF} = 0.035 \gamma_{ISF} (1 - \text{Hct}) \quad (11)$$

This assumes that there is no binding of glucose in the ISF space and that all of the ISF is freely accessible to the glucose. The estimates of  $V'_{ISF}$  averaged  $0.19 \pm 0.04$  ( $n = 18$ ) for the dog hearts and  $0.31 \pm 0.03$  ( $n = 23$ ) for the rabbit hearts. For comparison, an estimate of the total extracellular space of 19% or 0.179 ml/g was obtained by Polimeni (25) using sulfate in quickly frozen hearts from intact rats. Guller et al. (11) found a value of 0.21 ml/g to be their best estimate of  $V'_{ISF}$  in blood-perfused isolated dog hearts. Unpublished data from our own laboratory on  $V'_{ISF}$  for sucrose and cobaltic EDTA in anaesthetized intact rabbit hearts quickly frozen in their in vivo state averaged  $0.21 \pm 0.032$  ml/g ( $n = 432$ ). Thus the estimates obtained from the dog heart data from the modeling in our present study agree reasonably well with data obtained in vivo and from isolated blood-perfused hearts and again affirm the reasonableness of using a  $V_C$  of 0.035 ml/g to estimate the other spaces. As for the Tyrode-perfused rabbit hearts, it is clear that they become swollen because of the absence of albumin from the perfusate, and the values for  $\gamma_{ISF}$  are significantly higher. Our values for  $V'_{ISF}$  of  $0.30 \pm 0.03$  ml/g ( $n = 26$ ) are not as high as those of Schafer and Johnson (32) of 0.42 ml/g for total sucrose space, from which the estimated capillary plasma space should be subtracted. This is in spite of the fact that our perfusion system for the isolated rabbit hearts is fairly similar to what they used. The difference may be that we avoided any perfusion at high pressures which causes the hearts to swell more.

### Estimation of $PS_{pc}$ for D-glucose and Deoxyglucose

Values of  $PS_{pc}$  are high enough that reflux of untransformed tracer from cells occurs, which is to say that the intracellular concentration is above zero. Our estimates are based on the assumption that L-glucose serves as an extracellular reference that is not taken up by the

cells. The stereospecificity of the glucose transport system was demonstrated clearly by LeFevre and Marshall (15) and by Park et al. (22). As reviewed by these authors, the dextroglucoses exhibit the behavior expected of a carrier transport mechanism, i.e., inhibition, competition, and countertransport. The process is also facilitated by insulin and by anoxia, as reviewed by Morgan et al. (19), who also observed that the volume of distribution of L-glucose was not significantly different from that of an inert molecule, sorbitol. While they apparently did not test the effects of L-glucose on counter flow of nonmetabolized glucose analogues, they did observe an acceleration of D-glucose transport by insulin or anoxia when there was no effect on L-glucose transport.

The estimates of  $PS_{pc}$ , are compatible with the maximal glucose uptake rates of  $2 \mu\text{mol}\cdot\text{g}^{-1}\cdot\text{min}^{-1}$  in isolated Krebs-Henseleit-perfused rat hearts without insulin, in reports summarized by Randle and Tubbs (27). The transcapillary and transsarcolemmal fluxes must both exceed that by much of an order of magnitude to allow consumption at this rate and also the return of some tracer to the efflux as D-glucose. The transmembrane unidirectional fluxes  $J$  are given by  $J = PS \cdot C$ , where  $C$  is the concentration on the side of origin of the flux. With  $C_C$  equal to 5 mmol and  $PS_C$  equal to  $0.8 \text{ ml}\cdot\text{g}^{-1}\cdot\text{min}^{-1}$ , the unidirectional flux across the capillary wall would be  $4 \mu\text{mol}\cdot\text{g}^{-1}\cdot\text{min}^{-1}$ , which is more than adequate. Calculating a combined or total  $PS_T$  for transport across capillary and sarcolemmal membranes in series,  $PS_T = 1/(1/PS_C + 1/PS_{pc}) = 1/(1/0.8 + 1/0.5) = 0.29 \text{ ml}\cdot\text{g}^{-1}\cdot\text{min}^{-1}$  gives a maximum flux at a normal glucose concentration of 5 mM of  $5 \times 0.29 = 1.5 \mu\text{mol}\cdot\text{g}^{-1}\cdot\text{min}^{-1}$ , which is again adequate and exceeds normal metabolic utilization. However, a heart undergoing work stress and lacking fatty acid as a substrate would have greater demands, and delivery of glucose might well be transport limited unless  $PS_{pc}$  increased to compensate.

### Intracellular Reaction

While it is evident that to estimate  $G_{pc}$ , accurately the experimental data must be acquired with higher accuracy and for longer periods than was accomplished in these experiments, an interpretation of  $G_{pc}$  is nevertheless worthwhile. Conservation requires that the consumption be defined by the flow times the arteriovenous difference in the steady state, as well as by the intracellular reaction; therefore

$$F_S (C_{art} - C_{vein}) = G_{pc} C_{pc} \quad (12)$$

The unidirectional fluxes at the membranes must exceed this, as discussed in the previous section, i.e.,

$$\left. \begin{array}{l} PS_C C_C \\ \text{and} \\ PS_{pc} C_{ISF} \end{array} \right\} > PS_T C_C \geq G_{pc} C_{pc} \quad (13)$$

Taking values of  $F_S$  of  $1 \text{ ml}\cdot\text{g}^{-1}\cdot\text{min}^{-1}$  and  $C_{art} - C_{vein} = 0.2 \text{ mM}$ , then  $G_{pc} C_{pc} = 0.2 \mu\text{mol}\cdot\text{g}^{-1}\cdot\text{min}^{-1}$ . If  $G_{pc}$  were actually  $0.2 \text{ ml}\cdot\text{g}^{-1}\cdot\text{min}^{-1}$ , then  $C_{pc}$  would be 1 mM. Using Eq. 13 with  $C_C = 5 \text{ mM}$ , then  $PS_T$  should be  $G_{pc} \cdot C_{pc} / C_C = 0.2 G_{pc}$ . This inequality is fulfilled with values of  $G_{pc}$  as high as  $1.45 \text{ ml}\cdot\text{g}^{-1}\cdot\text{min}^{-1}$  even if  $PS_T$  is only  $0.29 \text{ ml}\cdot\text{g}^{-1}\cdot\text{min}^{-1}$ , as calculated in the preceding paragraph.

In the steady state, several features of the system must show compatibility: the consumption is measured by  $F_S(C_{art} - C_{vein})$ , by the intracellular consumption  $G_{pc} \cdot C_{pc}$  and by the net flux from blood into cell. If there is 3% arteriovenous extraction (the value obtained in 2 rabbit hearts) at a flow of  $2 \text{ ml}\cdot\text{g}^{-1}\cdot\text{min}^{-1}$ , the D-glucose consumption is  $2 \text{ ml}\cdot\text{g}^{-1}\cdot\text{min}^{-1} \times 5 \text{ mM} \times 0.03$  or  $0.3 \mu\text{mol}\cdot\text{g}^{-1}\cdot\text{min}^{-1}$ . The net intracellular reaction must match this exactly

(assuming no net flux into or from glycogen), so that  $C_{pc} = \text{consumption}/G_{pc} = 0.3 \mu\text{mol}\cdot\text{g}^{-1}\cdot\text{min}^{-1}/0.2 \text{ ml}\cdot\text{g}^{-1}\cdot\text{min}^{-1} = 1.5 \text{ mM}$ . The conductance from capillary lumen to inside the cell must be high enough to allow this consumption, so that the value  $PS_T \cdot (C_C - C_{pc})$  must exceed  $0.3 \mu\text{mol}\cdot\text{g}^{-1}\cdot\text{min}^{-1}$ , where  $PS_T$  is the overall conductance. If  $C_C - C_{pc} = 5 - 1.5 = 3.5 \text{ mM}$ , then  $PS_T$  must exceed  $0.3/3.5$  or  $0.1 \text{ ml}\cdot\text{g}^{-1}\cdot\text{min}^{-1}$ . With  $PS_C = 0.7$  and  $PS_{pc} = 0.6 \text{ ml}\cdot\text{g}^{-1}\cdot\text{min}^{-1}$ ,  $PS_T = 1/(1/0.6 + 1/0.7) = 0.32 \text{ ml}\cdot\text{g}^{-1}\cdot\text{min}^{-1}$ , a threefold excess over the minimal required conductance. This  $PS_T$  would permit a unidirectional flux  $PS_T(C_C - C_{pc})$  of  $0.32 \times 3.5 = 1 \mu\text{mol}\cdot\text{g}^{-1}\cdot\text{min}^{-1}$ . The conclusion is that the membrane barriers are only a mild impedance to glucose transport, and the permeabilities are high enough that bidirectional fluxes must occur, i.e., back diffusion, at both membranes. Insulin availability can be expected to raise,  $PS_{pc}$ , further.

Among the highest consumptions under insulin stimulation are the values reported by Penpargkul, Kuziak, and Scheuer (23) of  $0.67 \mu\text{mol}\cdot\text{g}^{-1}\cdot\text{min}^{-1}$  and by Rovetto, Whitmer, and Neely (30) of  $2 \mu\text{mol}\cdot\text{g}^{-1}\cdot\text{min}^{-1}$ . In the latter studies on Tyrode-perfused hearts the perfusate glucose level was  $22 \text{ mM}$ , so that the minimum  $PS_T$  had only to exceed  $0.09 \text{ ml}\cdot\text{g}^{-1}\cdot\text{min}^{-1}$  to allow the observed flux, presuming that  $G_{pc}$  was also increased in this stimulated situation where the insulin level was  $25 \text{ mU/ml}$ . They estimated that  $C_{pc}$  might be  $21 \text{ mM}$ , so that with  $C_C$  equal to  $22 \text{ mM}$ , the minimum  $PS_T$  would have to be  $2 \mu\text{mol}\cdot\text{g}^{-1}\cdot\text{min}^{-1}/1 \mu\text{mol}\cdot\text{ml}^{-1} \approx 2 \text{ ml}\cdot\text{g}^{-1}\cdot\text{min}^{-1}$  and  $G_{pc}$  could be as low as  $0.1 \text{ ml}\cdot\text{g}^{-1}\cdot\text{min}^{-1}$ . The high  $PS_T$  could be explained if insulin stimulation increased  $PS_{pc}$ , but capillary  $PS_C$  at the level observed in our rabbit hearts would be at a borderline level.

### $G_{pc}$ and its Relationship to the Glycolytic Series

The clearance or the “first-order sequestration process” may provide a measure of the rate of metabolic reaction so long as there is no further diffusional resistance inside the cell. Naturally, the first reaction in the series, the hexokinase reaction in which glucose is phosphorylated to glucose 6-phosphate, is a prime candidate. The reverse reaction, catalyzed by glucose-6-phosphatase is considered to be slow, if it occurs at all in the heart. The formation of fructose 6-phosphate via isomerase is not paralleled by a similar reaction for 2-deoxy-D-glucose because the transformation requires the availability of an -OH group in the two position. Thus 2-deoxy-D-glucose tends to be retained in the cell as the -6-phosphate unless dephosphorylated and cannot be further metabolized or stored as glycogen. Of consequence to the interpretation of images of [ $^{11}\text{C}$ ]2-deoxy-D-glucose obtained by positron emission tomography is the likelihood of washout from the cell rather than 100% retention in the phosphorylated form. Given that  $PS_{pc}$  and  $G_{pc}$  are similar for D-glucose and 2-deoxy-D-glucose and that phosphatase action is negligible, then the rate of uptake into 2-deoxyglucose-6-phosphate is related to the hexokinase reaction but is nevertheless dominated by flow and membrane transport. To interpret uptake data in terms of the hexokinase reaction, one must have good estimates of  $F_{S_p}$ ,  $PS_C$  and  $PS_{pc}$ , and of  $V'_{pc}$ .

$G_{pc}$  would represent the hexokinase reaction exactly in the absence of dephosphorylation or other reactions of glucose 6-phosphate or deoxyglucose 6-phosphate. However, for glucose, if the hexokinase and glucose 6-phosphatase reactions were both rapid compared with the further metabolic reactions (via hexosephosphate isomerase, phosphoglucomutase, or glucose-6-phosphate dehydrogenase), then the specific activity of the glucose 6-phosphate pool would rise so that there would be tracer return to the free glucose pool (mathematically equivalent to back diffusion); this effect of tracer return to the glucose increases with time at a rate inversely proportional to the pool size of glucose 6-phosphate.

These arguments demonstrate some of the difficulties in deriving kinetic interpretations from observations of multiple indicator-dilution curves, even with carefully chosen sets of

glucose analogues, and lead us to conclude that observations on the retention of a tracer such as [ $^{18}\text{F}$ ]2-deoxy-D-glucose, are similarly handicapped. A compartmental approach to interpreting the regional deposition of labeled glucoses in brain was worked out by Raichle et al. (26) and by Sokoloff et al. (33) in terms of the chemical reactions but omitting consideration of the influences of flow and of permeation through the capillary and cell membranes. Our present study demonstrates the permeation strongly influences the intracellular availability of glucose but is not the sole determinant of consumption rate. We would therefore hazard the warning that interpreting the rates of local tracer deposition as the measure of the rates of glucose metabolism, independent of flow and permeation, is inaccurate and that estimates of flow and particularly of permeabilities (which requires knowing flow) should be made and their influences taken into account. It is probably impossible to do this with observations of a single tracer, so multiple tracer studies should be devised for such situations. Moreover, the rate of glucose entry into the cell is equal to the rate of glycolysis only if there is no reflux of glucose from the cell and no incorporation into glycogen or activity of the hexose monophosphate shunt, so we conclude that tracer uptake normally overestimates the rate of glycolysis.

## Acknowledgments

Marta Chaloupka, Joseph Chan, and Craig Althen assisted with the data analysis and the illustrations and Geraldine Crooker with the manuscript preparation.

This work was supported by National Heart, Lung, and Blood Institute Grants HL-19135 and HL-19139 and by National Institutes of Health Division of Research Resources Grant RR-01243. J. Kuikka was supported by Fogarty International Fellowship TW-02480-01 from the National Institutes of Health.

## References

1. Alvarez OA, Yudilevich DL. Heart capillary permeability to lipid-insoluble molecules. *J. Physiol. Lond.* 1969; 202:45–58. [PubMed: 5770913]
2. Bassingthwaite JB. A concurrent flow model for extraction during transcapillary passage. *Circ. Res.* 1974; 35:483–503. [PubMed: 4608628]
3. Bassingthwaite JB.; Goresky, CA. *Handbook of Physiology. The Cardiovascular System. Microcirculation. Vol. 4. Am. Physiol. Soc.; Bethesda, MD: 1984. Modeling in the analysis of solute and water exchange in the microvasculature.; p. 549-626.sect. 2*chapt. 13
4. Bassingthwaite JB, Kuikka JT, Chan IS, Arts T, Reneman RS. A comparison of ascorbate and glucose transport in the heart. *Am. J. Physiol.* 1985; 249:H141–H149. *Heart Circ. Physiol.* 18. [PubMed: 3893161]
5. Bassingthwaite JB, Lenhoff AM, Stephenson JL. A sliding-element algorithm for rapid solution of spatially distributed convection-permeation models (Abstract). *Biophys. J.* 1984; 45:175a. [PubMed: 6324901]
6. Bassingthwaite JB, Yipintsoi T, Harvey RB. Microvasculature of the dog left ventricular myocardium. *Microvasc. Res.* 1974; 7:229–249. [PubMed: 4596001]
7. Cousineau D, Rose CP, Lamoureux D, Goresky CA. Changes in cardiac transcapillary exchange with metabolic coronary vasodilation in the intact dog. *Circ. Res.* 1983; 53:719–730. [PubMed: 6357532]
8. Crone C. Facilitated transfer of glucose from blood into brain tissue. *J. Physiol. Lond.* 1965; 181:103–113. [PubMed: 5866278]
9. Crone C, Thompson AM. Comparative studies of capillary permeability in brain and muscle. *Acta Physiol. Scand.* 1973; 87:252–260. [PubMed: 4718208]
10. Duran WN, Yudilevich DL. Estimate of capillary permeability coefficients of canine heart to sodium and glucose. *Microvasc. Res.* 1978; 15:195–205. [PubMed: 661611]

11. Guller B, Yipintsoi T, Orvis AL, Bassingthwaighe JB. Myocardial sodium extraction at varied coronary flows in the dog: estimation of capillary permeability by residue and outflow detection. *Circ. Res.* 1975; 37:359–378. [PubMed: 1098804]
12. Hawkins RA, Mans AM, Davis DW, Viña JR, Hibbard LS. Cerebral glucose use measured with [<sup>14</sup>C]glucose labeled in the 1, 2, or 6 position. *Am. J. Physiol.* 1985; 248:C170–C176. *Cell Physiol.* 17. [PubMed: 3881042]
13. King, RB.; Bassingthwaighe, JB. Radioactivity.. In: Reneman, RS.; Strackee, J., editors. *Data in Medicine: Collection, Processing and Presentation. Instrumentation and Techniques in Clinical Medicine.* Vol. I. Nijhoff; The Hague, Netherlands: 1979. p. 79-113.
14. King RB, Bassingthwaighe JB, Hales JRS, Rowell LB. Stability of heterogeneity of myocardial blood flow in normal awake baboons. *Circ. Res.* 1985; 57:285–295. [PubMed: 4017198]
15. LeFevre PG, Marshall JK. Conformational specificity in a biological sugar transport system. *Am. J. Physiol.* 1958; 194:333–337. [PubMed: 13559473]
16. Lenhoff AM, Lightfoot EN. The effects of axial diffusion and permeability barriers on the transient response of tissue cylinders. II. Solution in time domain. *J. Theor. Biol.* 1984; 106:207–238. [PubMed: 6369004]
17. Levin M, Kuikka J, Bassingthwaighe JB. Sensitivity analysis in optimization of time-distributed parameters for a coronary circulation model. *Med. Prog. Technol.* 1980; 7:119–124. [PubMed: 7393171]
18. Macchia DD, Page E, Polimeni PI. Interstitial anion distribution in striated muscle determined with [<sup>35</sup>S]sulfate and [<sup>3</sup>H]sucrose. *Am. J. Physiol.* 1979; 237:C125–C130. *Cell Physiol.* 6. [PubMed: 112873]
19. Morgan HE, Regen DM, Park CR. Identification of a mobile carrier-mediated sugar transport system in muscle. *J. Biol. Chem.* 1964; 239:369–374. [PubMed: 14169132]
20. Opie LH. Effects of regional ischemia on metabolism of glucose and fatty acids: relative rates of aerobic and anaerobic energy production during myocardial infarction and comparison with effects of anoxia. *Circ. Res., Suppl. I.* 1976; 38:I–52-I-74.
21. Paris S, Pouysselgur J, Ailhaud G. Analysis by counter-transport, relationship to phosphorylation and effect of glucose starvation. *Biochim. Biophys. Acta.* 1980; 602:644–652. [PubMed: 7437426]
22. Park CR, Rinewein D, Henderson MJ, Cadenas E, Morgan HE. The action of insulin on the transport of glucose through the cell membrane. *Am. J. Med.* 1959; 26:674–684. [PubMed: 13649694]
23. Penpargkul S, Kuziak J, Scheuer J. Effect of uremia upon carbohydrate metabolism in isolated perfused rat heart. *J. Mol. Cell. Cardiol.* 1975; 7:499–511. [PubMed: 1152075]
24. Phelps ME, Hoffman EJ, Huang SC, Kuhl DE. Positron tomography: in vivo autoradiographic approach to measurement of cerebral hemodynamics and metabolism. *Acta Neurol. Scand, Suppl.* 1977; 56:446–447. [PubMed: 268867]
25. Polimeni PI. Extracellular space and ionic distribution in rat ventricle. *Am. J. Physiol.* 1974; 227:676–683. [PubMed: 4413398]
26. Raichle ME, Larson KB, Phelps ME, Grubb RL Jr, Welch MJ, Ter-Pogossian MM. In vivo measurement of brain glucose transport and metabolism employing glucose-<sup>11</sup>C. *Am. J. Physiol.* 1975; 228:1936–1948. [PubMed: 1155625]
27. Randle, PJ.; Tubbs, PK. *Handbook of Physiology. The Cardiovascular System. The Heart.* Vol. 1. Am. Physiol. Soc.; Bethesda, MD: 1979. Carbohydrate and fatty acid metabolism.; p. 805-844.sect. 2chapt. 23
28. Rose CP, Goresky CA. Vasomotor control of capillary transit time heterogeneity in the canine coronary circulation. *Circ. Res.* 1976; 39:541–554. [PubMed: 786495]
29. Rose CP, Goresky CA, Bach GG. The capillary and sarcolemmal barriers in the heart. An exploration of labeled water permeability. *Circ. Res.* 1977; 41:515–533. [PubMed: 902358]
30. Rovetto MJ, Whitmer JT, Neely JR. Comparison of the effects of anoxia and whole heart ischemia on carbohydrate utilization in isolated working rat hearts. *Circ. Res.* 1973; 32:699–711. [PubMed: 4715192]

31. Sacks W, Schechter DC, Sacks S. A difference in the in vivo cerebral production of [ $1\text{-}^{14}\text{C}$ ]lactate from D-[ $3\text{-}^{14}\text{C}$ ]glucose in chronic mental patients. *J. Neurosci. Res.* 1981; 6:225–236. [PubMed: 6787210]
32. Schafer D, Johnson JA. Permeability of mammalian heart capillaries to sucrose and insulin. *Am. J. Physiol.* 1964; 206:985–991. [PubMed: 14208975]
33. Sokoloff L, Reivich M, Kennedy C, des Rosiers MH, Patlak CS, Pettigrew KD, Sakurada O, Shinohara M. The [ $^{14}\text{C}$ ]deoxyglucose method for the measurement of local cerebral glucose utilization: theory, procedure, and normal values in the conscious and anesthetized albino rat. *J. Neurochem.* 1977; 28:897–916. [PubMed: 864466]
34. Yipintsoi T. Single-passage extraction and permeability estimation of sodium in normal dog lungs. *Circ. Res.* 1976; 34:523–531. [PubMed: 786494]
35. Yipintsoi T, Bassingthwaighte JB. Circulatory transport of iodoantipyrine and water in the isolated dog heart. *Circ. Res.* 1970; 27:461–477. [PubMed: 5452741]
36. Yipintsoi T, Dobbs WA, Scanlon PD, Knopp TJ, Bassingthwaighte JB. Regional distribution of diffusible tracers and carbonized microspheres in the left ventricle of isolated dog hearts. *Circ. Res.* 1973; 33:573–587. [PubMed: 4752857]
37. Yipintsoi T, Scanlon PD, Bassingthwaighte JB. Density and water content of dog ventricular myocardium. *Proc. Soc. Exp. Biol. Med.* 1972; 141:1032–1035. [PubMed: 4645751]
38. Yipintsoi, T.; Tancredi, RG.; Richmond, DR.; Bassingthwaighte, JB. Myocardial extractions of sucrose, glucose, and potassium. In: Crone, C.; Lassen, NA., editors. *Capillary Permeability. Proceedings of Alfred Benzon Symposium II.* Munksgaard; Copenhagen: 1970. p. 153-156.
39. Yudilevich DL, De Rose N. Blood-brain transfer of glucose and other molecules measured by rapid indicator dilution. *Am. J. Physiol.* 1971; 220:841–846. [PubMed: 4925747]

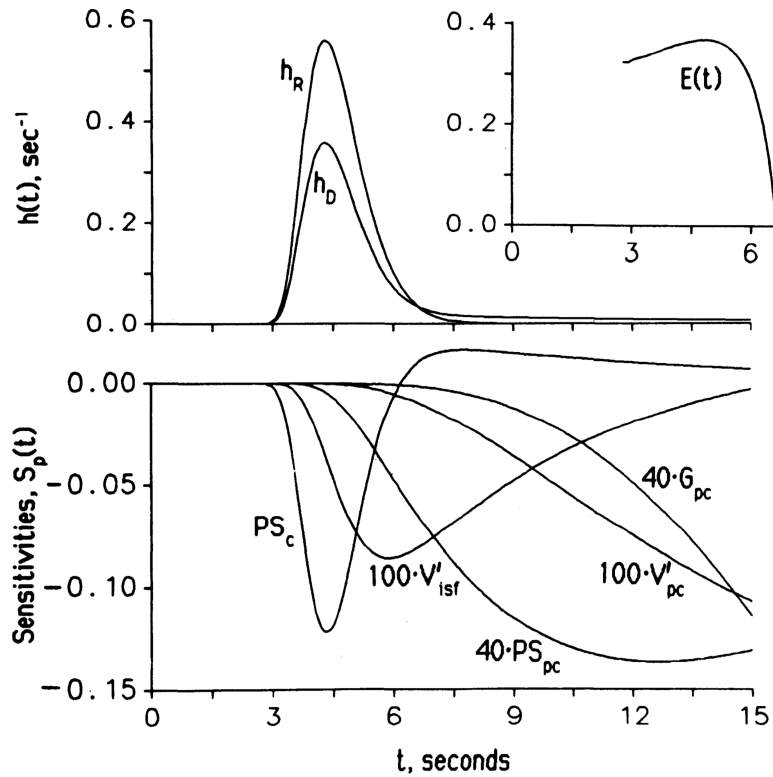


**Fig. 1.**

Impulse responses and sensitivity functions ( $S$ ) for a capillary interstitial fluid (ISF)-cell model solution with parameter values suitable for D-glucose in the heart. Notice that sensitivity functions are all different, indicating independence of the parameters in shaping model solutions. Note too that  $V'_{pc}$  and  $G_{pc}$  have little influence at early times and more later, suggesting the importance of avoiding (or accounting for) recirculation. Parameter values used to generate model solutions were 7-path model with relative dispersion of flows = 30%;  $F_s = 1.5 \text{ ml}\cdot\text{g}^{-1}\cdot\text{min}^{-1}$ ;  $PS_c$  and  $PS_{pc} = 0.75$  and  $0.5 \text{ ml}\cdot\text{g}^{-1}\cdot\text{min}^{-1}$ ;  $G_{pc} = 0.5 \text{ ml}\cdot\text{g}^{-1}\cdot\text{min}^{-1}$ ;  $\gamma_{pc}$  (which is  $V'_{pc}/V'_c$ ) = 10, and  $\gamma_{ISF}$  (which is  $V'_1/V'_c$ ) = 5. (Input function is a gamma variate function with a mean transit time of 3 s, a relative dispersion of 0.2, and a skewness of 1.0.) Scalar multiplier of 40  $S_{PS_{pc}}$  and  $S_{G_{pc}}$  and of 100 for  $S_{V'_{IST}}$  and  $S_{V'_{pc}}$  indicate that sensitivity to  $PS_c$  is higher than to any other parameter. Units of  $S$ ,  $\text{s}^{-1}/(\text{units of parameter})$ . See text for abbreviations.

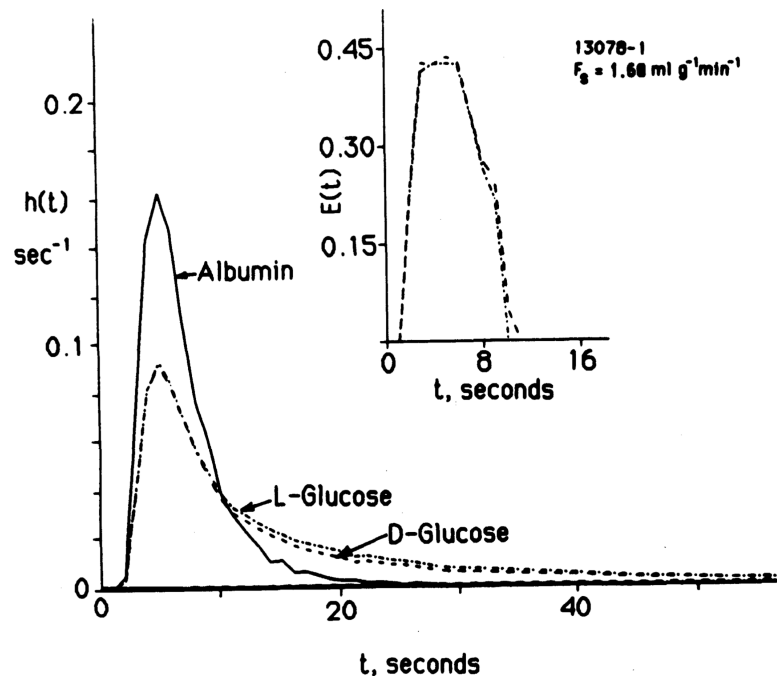


**Fig. 2.** Coronary sinus outflow dilution curves for D- and L-glucose in a rabbit heart after injection of tracers into the aortic cannula at  $t = 0$ . Main peaks of impulse responses for D- and L-glucose are nearly identical. Extraction curves,  $E(t)$  in *insert*, provide a more critical test of their similarity and show the same result. Tail of D-glucose curve is lower than that of L-glucose, in accord with uptake by myocardial cells. (Expt no. 13078-1. Data given in numerical form in Table 3.)

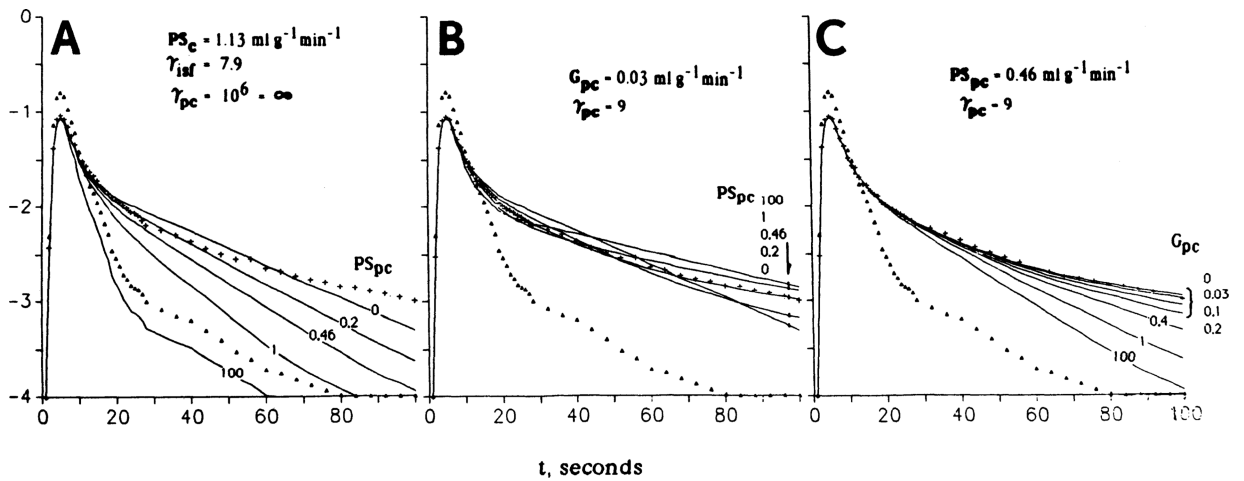


**Fig. 3.**

Multicapillary solutions for a capillary interstitial fluid (ISF)-cell-reaction model of D-glucose outflow dilution curves from same Krebs-Ringer perfused rabbit heart as in Fig. 2 (no. 13078-1). *A*: solutions for a reduced model for capillary permeation and cellular uptake without return flux from cell but with return flux from ISF to capillary. Heterogeneity of flows was approximated using 7 parallel pathways with a Gaussian distribution of flows with relative dispersion 30%. Five solutions are drawn for different values of the rate of cellular influx ( $PS_{pc}$ ), all other parameters being constant.  $F_s = 1.68 \text{ ml}\cdot\text{g}^{-1}\cdot\text{min}^{-1}$ ;  $PS_c = 1.13 \text{ ml}\cdot\text{g}^{-1}\cdot\text{min}^{-1}$ ;  $\gamma_{pc} = 7.9$ ;  $\gamma_{pc} = \infty$ , to prevent reflux from the cell. *B*: effects of cellular permeation, now with return flux from cell to ISF. Intracellular consumption,  $G_{pc} = 0.03 \text{ ml}\cdot\text{g}^{-1}\cdot\text{min}^{-1}$ ; other parameters same as for *A*. Best fit is obtained with  $PS_{pc} = 0.42 \text{ ml}\cdot\text{g}^{-1}\cdot\text{min}^{-1}$  and  $\gamma_{pc} = 9$ . *C*: effect of  $G_{pc}$  on shapes of tails of outflow dilution curves. Increasing rates of consumption reduce reflux from cell into outflow, lowering tails of curves. Best fit values were  $PS_c = 1.13 \text{ ml}\cdot\text{g}^{-1}\cdot\text{min}^{-1}$ ,  $\gamma_{ISF} = 7.9$ ,  $PS_{pc} = 0.46 \text{ ml}\cdot\text{g}^{-1}\cdot\text{min}^{-1}$ ,  $\gamma_{pc} = 9$ , and  $G_{pc} = 0.03 \text{ ml}\cdot\text{g}^{-1}\cdot\text{min}^{-1}$ . When  $PS_{pc}$  is higher, sensitivity to  $G_{pc}$  is higher. (Numerical values of data points and of model solutions are listed in Table 3.)

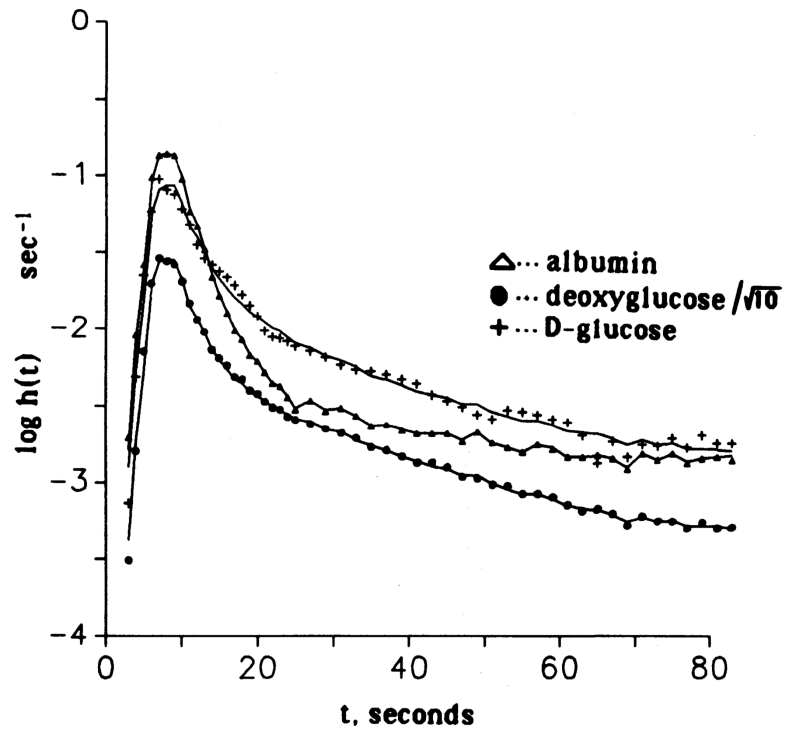


**Fig. 4.** Outflow dilution curves for D-glucose and deoxyglucose and albumin (dog expt 4048-6) fitted with the model. Deoxyglucose curve is shifted downward by half a logarithmic decade (ordinate values divided by  $10^{1/2}$ ) to display it separately from D-glucose curve. Parameter estimates logarithmic for D- and deoxyglucose were  $PS_c$ , 0.97 and 1.0;  $PS_{pc}$  = 0.7 and 0.5;  $G_{pc}$ , = 0.01 and 0.05  $\text{ml}\cdot\text{g}^{-1}\cdot\text{min}^{-1}$ ;  $\gamma_{ISF}$  = 6.5 and  $\gamma_{pc}$  = 13.3  $\text{ml/g}$  for both. Coefficients of variation were 0.19 and 0.09.

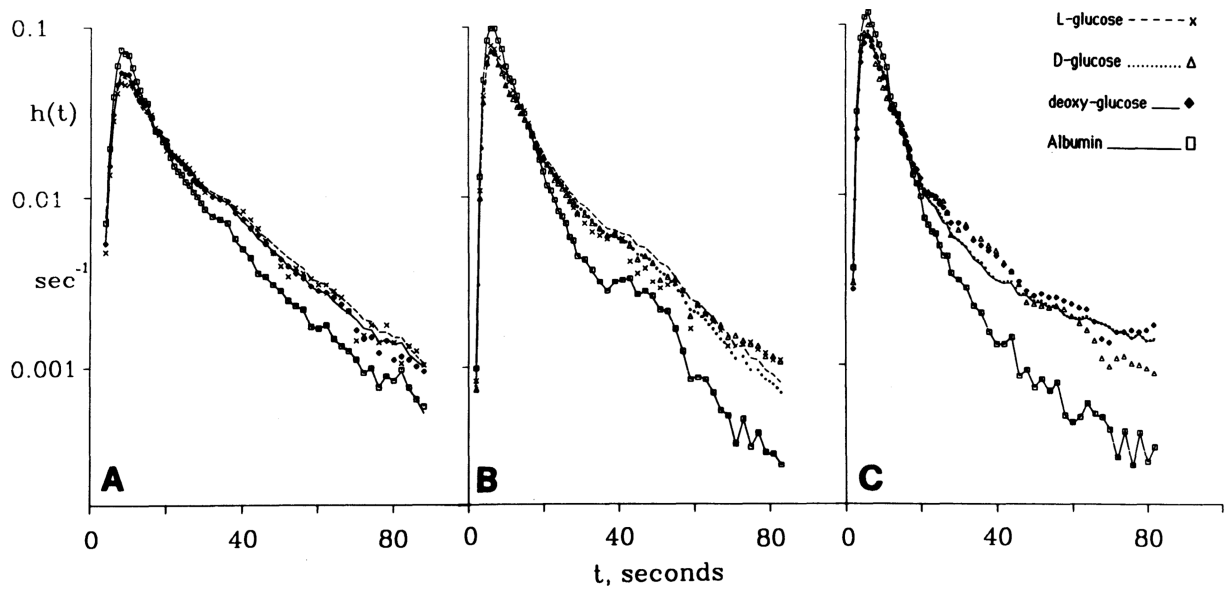


**Fig. 5.**

Constrained fitting of a capillary interstitial-fluid (ISF)-cell-reaction model to 9 coronary outflow dilution curves for albumin, D-, L-, and 2-deoxy-D-glucose. (Expts 30284, 2, and 3.) *Symbols* are data points; *lines* give model solutions fitted to data under strong constraints. Regional flows were from microsphere deposition densities. The only free parameters were 1 value each for  $PS_c$  and  $V'_{ISF}$  and 2 for  $PS_{pc}$  and for D- and 2-deoxy-D-glucose (see text). Since  $PS_c$  affects most strongly the first 20–30 s of the curves, result is excellent fitting of parts of curve sensitive to  $PS_c$  and poorer fitting tails at 30–80 s where  $V'_{ISF}$ ,  $PS_{pc}$ , and  $V'_{pc}$  have influences.

TABLE 1

Capillary and sarcolemmal permeabilities in isolated blood-perfused dog hearts

Expt No.	$F_s$ , ml·g <sup>-1</sup> ·min <sup>-1</sup>	RD, $\mu$ m	$P_{SC}$ , ml·g <sup>-1</sup> ·min <sup>-1</sup>		$\gamma_{ISF}$	$P_{PC}$ , ml·g <sup>-1</sup> ·min <sup>-1</sup>		$\gamma_{PC}$	CV	
			D-Glc	Deoxy-Glc		D-Glc	Deoxy-Glc		L-Glc	D-Glc
30127-1	0.53	0.37	0.49	0.3*	7.8	0.3*	12.5*	0.22	0.19	
30127-2	0.51	0.37	0.51	0.6*	6.0	0.6*	12.5*	0.36	0.20	
30127-3	0.49	0.54	0.45	0.3*	5.1	0.3*	12.5*	0.27	0.25	
30127-4	0.41	0.54	0.39	0.6*	4.0	0.6*	12.5*	0.36	0.39	
3028-1	1.48	0.28	0.76	0.2	4.2	0.2	9.8	0.11	0.04	
3028-2	1.48	0.28	0.75	0.5	4.7	0.5	12.8	0.18	0.10	
3028-3	1.47	0.28	0.71	0.8	7.0	0.8	12.6	0.23	0.06	
3028-4	1.52	0.3	0.62	0.1	3.7	0.1	12.9	0.13	0.12	
3028-5	1.62	0.3	0.60	0.4	4.0	0.4	12.9	0.12	0.13	
3028-6	1.64	0.3	0.65	0.3	5.0	0.3	14.0	0.22	0.27	
22028-1	1.72	0.30	0.81	0.3	5.2	0.3	12.5*	0.12	0.10	
22028-3	2.36	0.30	0.81	0.8	6.1	0.8	12.0	0.12	0.22	
4048-1	1.37	0.56	0.91	0.1	3.9	0.1	12.9	0.14	0.06	
4048-2	1.28	0.56	0.82	0.5	4.4	0.5	13.0	0.11	0.20	
4048-3	1.07	0.56	0.96	0.6	6.6	0.6	14.8	0.073	0.05	
4048-4	1.66	0.49	1.30	0.4	7.4	0.4	12.5*	0.15	0.06	
4048-5	1.61	0.49	0.74	0.5	5.4	0.5	12.9	0.13	0.24	
4048-6	1.36	0.49	0.97	0.7	6.5	0.7	13.3	0.19	0.08	
Mean	1.31	0.41	0.72	0.80	5.4	0.57	12.7	0.18	0.19	0.12
$\pm$ SD	$\pm 0.51$	$\pm 0.11$	$\pm 0.17$	$\pm 0.22$	$\pm 1.25$	$\pm 0.15$	$\pm 0.94$	$\pm 0.087$	$\pm 0.083$	$\pm 0.081$
<i>n</i>	18	18	11	12	18	11	12	13	11	12

$F_s$ , flow of solute-containing mother fluid; RD, relative dispersion;  $P_{SC}$  and  $P_{PC}$ , permeability-surface area product of capillaries and parenchymal cells, respectively;  $\gamma_{ISF}$  and  $\gamma_{PC}$ , dimensionless ratios of interstitial volume of distribution and of volume of tracer distribution; CV, coefficient of variation. Experiment numbers have animal number first, then run number. In individual runs for L-glucose,  $P_{SC}$  and  $\gamma_{ISF}$  were estimated jointly with a dextralucose.  $\gamma_{ISF}$  was also estimated jointly for the dextralucose runs. Values of  $P_{SC}$  and  $\gamma_{ISF}$  for L-glucose were obtained for each experiment, except where both D- and 2-deoxy-D-glucose were paired. Values for  $\gamma_{ISF}$  were identical to those of D-glucose or were 1.048 times that of 2-deoxy-D-glucose; average  $P_{SC}$  (L-Glc) was  $0.69 \pm 0.22$  ( $n = 13$ ). Estimates of infinite intracellular consumption averaged roughly  $0.2 \text{ ml}\cdot\text{g}^{-1}\cdot\text{min}^{-1}$  but were too imprecise to merit individual reporting.

\* Data not sufficiently accurate to permit estimation.

Watermark-text

Watermark-text

Watermark-text

**TABLE 2**

Capillary and sarcolemmal permeabilities in isolated Tyrode-perfused rabbit hearts

Expt No.	$F_s$ , ml·g <sup>-1</sup> ·min <sup>-1</sup>	RD, μm	$PS_C$ , ml·g <sup>-1</sup> ·min <sup>-1</sup>		$\gamma$ ISF	$PS_{pc}$ , ml·g <sup>-1</sup> ·min <sup>-1</sup>		$\gamma$ pc	CV	
			D-Glc	Deoxy-Glc		D-Glc	Deoxy-Glc		L-Glc	D-Glc
13078-1	1.7	0.30	1.1	1.1	7.9	0.4	0.4	9.0	0.098	0.092
13078-2	1.7	0.30	1.3	1.40	9.5	0.4	0.5	7.5	0.039	0.055
13078-3	1.7	0.44	1.3	1.3	9.0	0.42	0.42	9.0	0.079	0.061
13078-4	1.7	0.44	1.2	1.25	10.0	0.5	0.42	10.0	0.056	0.039
12068-1	2.8	0.3	1.0	1.0	8.5	0.6	0.6	13.0	0.19	
12068-2	2.4	0.3	1.0	1.04	9.0	0.3	0.16	12.0	0.18	0.17
Mean ± SD	2.0		1.15	1.23	9.0	0.45	0.36	10.1	0.09	0.08
<i>n</i>	±0.5		±0.14	±0.18	±0.7	±0.1	±0.18	±2.1	±0.06	±0.07
	23		23	3	23	23	3	23	2	3

Abbreviations as in Table 1.

TABLE 3

Example data set (13078-1) and model fit

Time, s	Albumin		<sup>14</sup> CIL-glucose		<sup>3</sup> HID-glucose	
	$\hat{h}_R$	$h_{D1}$	$\hat{h}_R$	$h_{D1}$	$\hat{h}_{D2}$	$h_{D2}$
1	10	20	10	155	10	155
2	5,129	5,754	3,802	5,888	3,802	5,888
3	75,857	81,283	42,658	40,738	41,687	40,738
4	147,910	151,355	81,283	79,432	83,176	79,432
5	165,958	165,958	91,201	93,325	91,201	93,325
6	151,355	147,910	83,176	85,113	83,176	85,113
7	112,201	109,647	69,183	69,183	69,183	69,183
8	79,432	77,624	56,234	54,954	56,234	54,954
9	63,095	61,659	46,773	45,708	45,708	44,668
10	39,810	38,904	38,904	36,308	37,153	34,673
11	30,903	30,903	33,113	30,903	30,903	29,512
12	23,442	23,442	30,199	27,542	27,542	25,704
13	17,783	17,378	26,302	23,988	23,988	22,387
14	14,791	14,454	23,442	21,877	21,877	19,952
15	11,481	11,481	21,379	20,417	19,498	17,783
16	9,332	9,120	19,054	18,621	16,982	15,849
17	6,918	6,761	17,783	16,982	15,488	14,454
18	5,370	5,370	16,596	15,849	14,125	12,882
19	3,715	3,548	15,488	14,454	12,882	11,749
20	3,020	3,020	14,454	13,489	12,023	10,715
21	2,570	2,512	13,489	12,882	11,220	10,000
22	2,089	2,042	12,589	12,023	10,471	9,332
23	1,820	1,778	11,749	11,481	9,772	8,710
24	1,549	1,549	10,471	10,965	8,912	8,128
25	1,445	1,445	10,471	10,471	8,710	7,762
26	1,380	1,380	9,550	10,000	8,128	7,413
27	1,288	1,288	8,511	9,550	7,244	6,918

Time, s	Albumin		<sup>14</sup> C]-L-glucose		<sup>3</sup> H]D-glucose	
	<i>h<sub>R</sub></i>	<i>h<sub>D</sub></i>	<i>h<sub>D1</sub></i>	<i>h<sub>D2</sub></i>	<i>h<sub>D1</sub></i>	<i>h<sub>D2</sub></i>
28	871	851	7,762	8,912	6,456	6,456
32	813	813	6,761	7,586	5,754	5,370
36	741	724	6,026	6,309	5,129	4,467
40	646	646	5,012	5,370	4,365	3,890
44	575	575	4,074	4,467	3,715	3,311
48	468	468	3,388	3,715	3,236	2,951
52	251	245	2,884	3,020	2,884	2,512
56	219	219	2,455	2,512	2,884	2,239
60	200	200	2,089	2,089	2,291	2,042
64	182	182	1,778	1,738	2,138	1,862
68	155	155	1,585	1,445	1,905	1,698
72	126	126	1,349	1,202	1,738	1,585
76	100	98	1,175	1,000	1,622	1,479
80	135	138	1,000	851	1,445	1,380
84	78	76	912	692	1,413	1,288
88	45	45	776	562	1,288	1,175
92	59	59	692	479	1,202	1,122
96	145	145	617	457	1,096	1,096
100	85	85	550	355	1,000	1,023
104	52	25	501	219	933	871
108	24	10	447	78	832	741
112	71		398	10	794	603
116	43		380		776	457
120	24		324		692	316
124	66		295		676	182
128	36		251		603	42
132	33		234		562	10
136	40		229		562	
140	29		209		537	
144	29		186		468	

\$watermark-text

\$watermark-text

\$watermark-text

$F_{\text{S}} = 1.68 \text{ ml}\cdot\text{g}^{-1}\cdot\text{min}^{-1}$ , Model parameters:  $P_{\text{S}}^{\text{D}}$  for D- and L-glucose =  $1.13 \text{ ml}\cdot\text{g}^{-1}\cdot\text{min}^{-1}$ ;  $\gamma_{\text{ISF}}$  for D- and L-glucose =  $7.94 \text{ ml/g}$ ;  $P_{\text{S}}^{\text{L}}$  for D-glucose =  $0.46 \text{ ml}\cdot\text{g}^{-1}\cdot\text{min}^{-1}$ , (zero for L-glucose);  $\gamma_{\text{PC}} = 9.0 \text{ ml/g}$ ;  $G_{\text{PC}} = 0.03 \text{ ml}\cdot\text{g}^{-1}\cdot\text{min}^{-1}$ . See also Figs. 2 and 3. The transport functions,  $h(t)$ , fraction per second are multiplied by  $10^6$ . Other abbreviations as in Table 1.